Eur. Phys. J. B **40**, 167–176 (2004)
DOI: 10.1140/epjb/e2004-00255-1

THE EUROPEAN PHYSICAL JOURNAL B

Two dimensional fluoride ion conductor $RbSn_2F_5$ studied by impedance spectroscopy and ^{19}F, ^{119}Sn, and ^{87}Rb NMR

K. Yamada[1], M.M. Ahmad[1,a], Y. Ogiso[1], T. Okuda[1], J. Chikami[2], G. Miehe[2], H. Ehrenberg[2], and H. Fuess[2]

[1] Department of Chemistry, Graduate School of Science, Hiroshima University, Kagamiyama 1-3-1, Higashi-Hiroshima 739-8526, Japan
[2] Institute for Materials Science, Darmstadt University of Technology, Petersenstrasse 23, 64287 Darmstadt, Germany

Received 4 April 2003 / Received in final form 25 May 2004
Published online 12 August 2004 –

Abstract. $RbSn_2F_5$ is a two-dimensional fluoride ion conductor. It undergoes a first-order phase transition to a superionic state at 368 K. The structure of the low temperature phase has been determined from the Rietveld analysis of the X-ray powder diffraction. The dynamic properties of the fluoride ions in $RbSn_2F_5$ have been studied by impedance spectroscopy and solid state NMR. The dc ionic conductivity of this sample shows an abrupt increase at the phase transition temperature. We have obtained the hopping frequency and the concentration of the charge carriers (F^- ions) at different temperatures from the analysis of the conductivity spectra using Almond-West formalism. The estimated values of the charge carriers' concentration agree well with that determined from the structure and were found to be independent of temperature. The relatively small value of the power-law exponent, $n \approx 0.55$, supports the two-dimensional property of the investigated material. Furthermore, ^{19}F NMR with simulation has suggested the diffusive motions of the fluoride ions between different sites. In contrast, ^{119}Sn and ^{87}Rb NMR spectra below 250 K supported the intrinsic disordered nature due to the random distribution of the fluoride ion vacancies.

PACS. 66.30.Hs Self-diffusion and ionic conduction in nonmetals – 77.22.Gm Dielectric loss and relaxation – 76.60.-k Nuclear magnetic resonance and relaxation

1 Introduction

Ionic and electronic conduction phenomena in disordered solids have attracted considerable interest from both experimentalists and theorists. The transport properties of ionic conductors depend largely upon the hopping dynamics of ionic charge carriers. Although the motion of ionic charge carriers has been examined using many different techniques, the two techniques most widely used are NMR [1,2] and conductivity measurements [3]. The frequency-dependent conductivity measures the macroscopic relaxation properties of the electric field and thus probes the dissipation due to the long-range diffusion of the charge carriers [4]. On the other hand, NMR relaxation probes the local charge density fluctuations and the activation energy determined from NMR experiments is often observed to be lower than that for the conductivity and corresponds to the local motion [1,5].

The real part of the ac conductivity of many ionic conducting materials exhibits a frequency dependence that is well approximated by a power-law of the form [6,7]

$$\sigma'(\omega) = \sigma_{\rm dc} + A\,\omega^n, \tag{1}$$

where $\sigma_{\rm dc}$ is the dc conductivity, A is a constant, ω is the angular frequency, and n is the power-law exponent describing the electrical relaxation behavior, mostly with $0.5 \leq n \leq 0.9$. The frequency independent dc conductivity $\sigma_{\rm dc}$ represents the random process in which the ions diffuse throughout the network by performing repeated hops between charge compensating sites. The power law dispersion, however, indicates a non-random process, wherein the ion motion is correlated. Since the exponent n ranges between 0.5 and 0.9, this correlation motion is sub-diffusive and indicates a preference on the part of ions that has hopped away to return to where it started.

However, considerably more prominent in the literature is the electric modulus formalism, $M^*(\omega) = 1/\varepsilon^*(\omega)$, where $\varepsilon^*(\omega)$ is the complex permittivity. The frequency dependence of $M^*(\omega)$ for ion conducting materials can be related to a corresponding time-dependent evolution of the electric field resulting from ion motions. Interesting controversy about which of the conductivity or electric modulus representations provides better insight into

[a] *Permanent address*: Physics Department, Faculty of Education, Assiut University in The New Valley, El-Kharga, Egypt
e-mail: mmahmad@sci.hiroshima-u.ac.jp

the relaxation process in ionic materials has surfaced over the years. Several researchers have noted discrepancies between interpretations drawn from the two analysis formalisms [8–10]. Recent examinations of the scaling properties of $\sigma^*(\omega)$ and $M^*(\omega)$ have shown disturbing differences [11–13]. For a given material, however, both $\sigma^*(\omega)$ and $M^*(\omega)$ exhibit linear scaling as a function of varying temperature, which means that $\sigma^*(\omega)$ or $M^*(\omega)$ spectra measured at various temperatures can be scaled so as to collapse to a single master curve.

$RbSn_2F_5$ has attracted considerable interest due to its high fluoride ion conductivity and has been characterized by dc conductivity and ^{19}F NMR spin lattice relaxation measurements [14,15]. $RbSn_2F_5$ belongs to MSn_2F_5-type compounds that found in the MF-SnF_2 pseudo-binary system, where M is a monovalent cation. While discrete complex ions, $[SnF_3]^-$ and $[Sn_2F_5]^-$, are recognized in NH_4SnF_3 and $NaSn_2F_5$ compounds, respectively, [16,17] no definite complex anions were recognized in $RbSn_2F_5$ compound. The crystal structure of $RbSn_2F_5$ was reported to be isomorphous with KSn_2F_5 with a trigonal structure ($P\overline{3}$, $Z = 3$) at room temperature [18]. Therefore, the two-dimensional anionic layer having vacant fluoride ion sites may contribute to the high ionic conductivity of this crystal. The crystal undergoes a first order phase transition to the superionic state at 368 K.

In this paper, we have studied the structure of the low temperature phase for $RbSn_2F_5$ and the conductivity spectra at different temperatures using the conductivity formalism. Almond-West formalism is used in the analysis of the conductivity spectra to determine the hopping frequency of mobile ions and the dc conductivity, and consequently enables us to estimate the values of the charge carriers' concentration at different temperatures. We have also studied ^{19}F, ^{119}Sn, and ^{87}Rb NMR spectra over a wide temperature range in order to explore the local structural changes in $RbSn_2F_5$.

2 Experimental

$RbSn_2F_5$ was prepared from aqueous solution according to Vilminot et al. [19]. Well developed crystals could be obtained under the hydrothermal condition at 440 K for several days. The thin plate precipitate of $RbSn_2F_5$ was then filtered off immediately, washed with water and dried in *vacuo*. The potassium analogue was also prepared by similar procedure. The product was characterized by X-ray powder diffraction using a Rigaku Rint PC diffractometer. Because of the strong preferred orientation of the powder, the diffraction data suitable for the Rietveld analysis was recorded using a STOE transmission type diffractometer with a Ge monochromatized Cu K_α radiation and a rotating flat plate sample. Data were collected with a PSD ($10 \leq 2\theta \leq 50°$). Structural parameters were refined by a Rietveld method [20].

Heat-flow type DSC measurements were performed using sealed glass tubes in the temperature range from 300 to 500 K at a heating rate of 4 K/min and the enthalpy changes at the transitions were calculated from the peak area. The enthalpy vs. peak area was calibrated in advance using a phase transition of KNO_3 at 401 K.

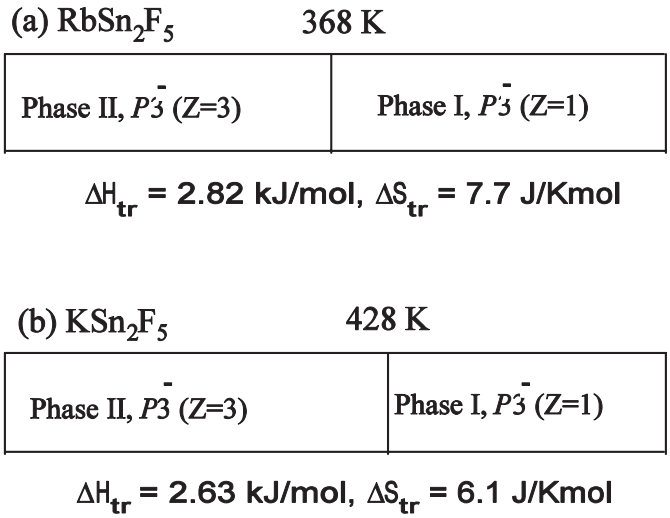

Fig. 1. Phase diagrams of $RbSn_2F_5$ and KSn_2F_5.

Impedance measurements were performed using a compressed powder pellet with carbon paints on both sides. The sample was then held between two spring-loaded electrodes. The impedance $|Z^*|$ and phase angle θ, were measured with a computer interfaced HIOKI 3532 LCR meter (42 Hz–5 MHz) in the temperature range from 200 to 450 K with a heating rate of 1 K/min. ^{19}F, ^{87}Rb and ^{119}Sn NMR spectra were observed at 6.4 T by means of a home-made pulsed spectrometer using a traditional single pulse sequence. The dead time of our spectrometer was 4–5 μs for all cases. The ^{19}F NMR spectrum simulation was performed using a Mathcad program developed by us [21].

3 Results and discussion

3.1 Phase transition and structure

The freshly prepared $RbSn_2F_5$ shows only one endothermic peak at 368 K (peak position) on heating. However, the thermal behavior of this Rb salt changed slowly with time and two weak endothermic peaks appear at 331 and 363 K after several months. In this paper, however, we will discuss only about the freshly prepared sample. Each phase of this sample was abbreviated as Phase I and II from the high temperature side as shown in Figure 1. Quite similar thermal behavior was observed for KSn_2F_5. Although two transitions was reported by Vilminot et al. for KSn_2F_5 [22], our freshly prepared sample showed only one endothermic peak at 428 K. Figure 1 summarizes these phase diagrams for Rb and K salts together with the thermodynamic parameters at the phase transitions.

The X-ray powder pattern for $RbSn_2F_5$ at Phase II suggests an isomorphous structure with the potassium salt and hence two possible space groups $P3$ (No. 143) and $P\overline{3}$ (No. 147). ^{87}Rb NMR is one of the suitable techniques to decide the correct space group, since three and

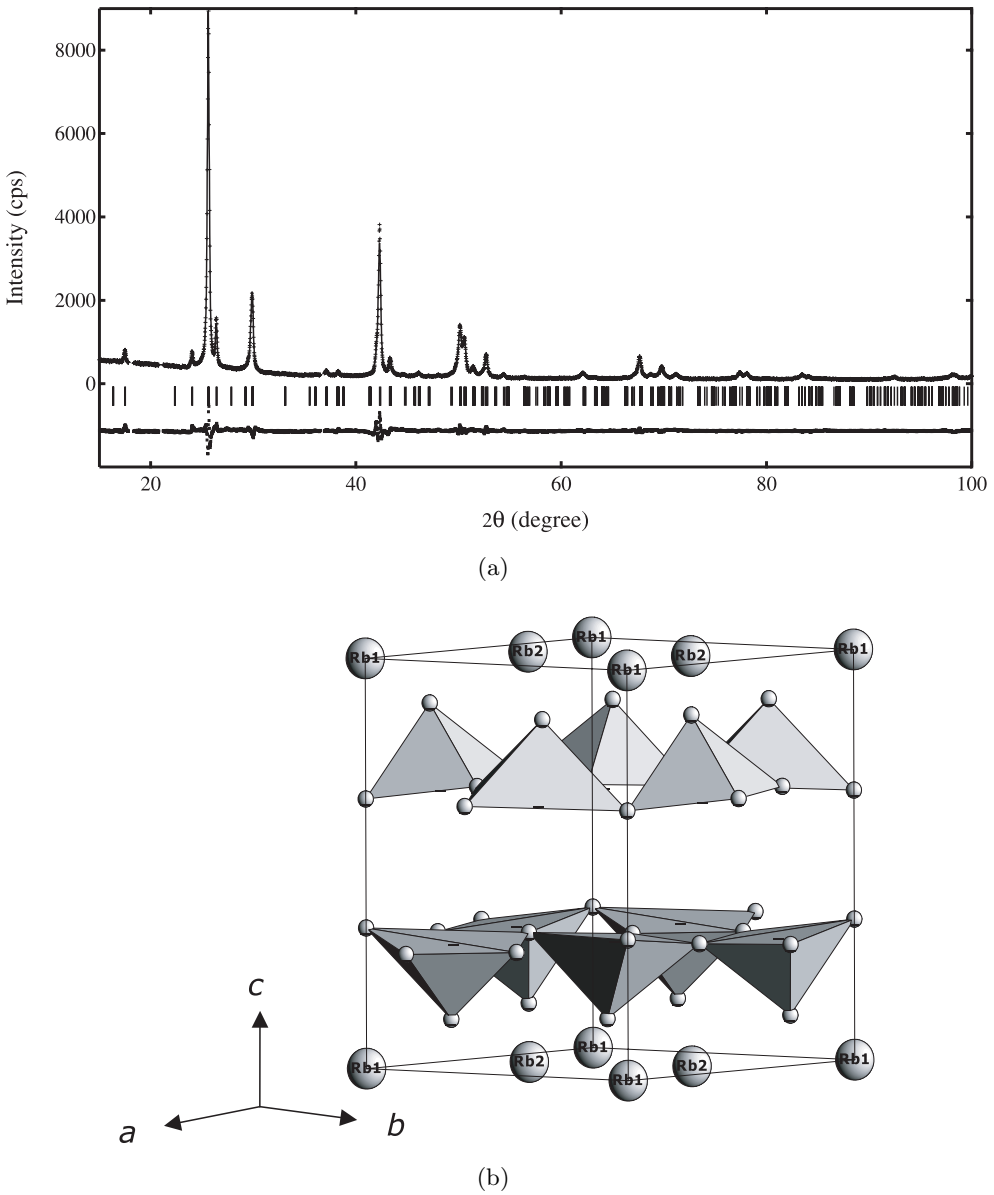

Fig. 2. (a) Final Rietveld refinement of $RbSn_2F_5$ at 295 K and (b) the structure of Phase II.

two crystallographic sites are expected for space group $P3$ and $P\overline{3}$, respectively. As will be stated later, however, the ^{87}Rb NMR below 250 K did not show clearly the number of the Rb sites probably due to the random distribution of the fluoride ion vacancies. Therefore, our Rietveld refinement was performed assuming a centrosymmetrical space group $P\overline{3}$. Figure 2 shows the final refinement plots together with the structure of Phase II (at 295 K). The refined lattice parameters and structural parameters are summarized in Table 1. Similar to the potassium salt, each Sn atom has a pseudo square-pyramidal coordination with one vertical short Sn-F1 bond (2.05(2) Å), two bridging Sn-F2 bonds (2.14(2) and 2.24(2) Å), and two triply bridging Sn-F3 (2.44(2) Å) and Sn-F4 (2.49(2) Å) bonds. In the Rietveld refinement the occupancy of the F1 site was fixed to 1.0 and those of the bridging and triply bridging F sites were assumed to be 0.9 in order to satisfy the stoichiometry. In this space group adjacent layers are equivalent related by a center of symmetry.

Although a strong endothermic peak was observed on the DSC curves, the X-ray powder pattern didn't show apparent changes at T_{tr}, except the disappearance of some weak reflections. These findings suggest the order-disorder property of the phase transition and also suggest the appearance of the averaged structure above T_{tr}. As Figure 1 shows, the entropy change at T_{tr} was estimated as $\Delta S_{tr} = 7.7\ \mathrm{J\,K^{-1}\,mol^{-1}}$ which was larger than that of KSn_2F_5. This entropy change corresponds to $R\ln(W_H/W_L)$ with $W_H/W_L = 2.5$, where W_H and W_L represent the number of microscopic states in the high- and low-temperature phases, respectively. Furthermore, an interesting change of the lattice constants at T_{tr} was observed as shown in

Table 1. (a) Lattice parameters of $RbSn_2F_5$ and (b) structural parameters at 295 K.

(a)

Temperature	295 K*	400 K
Space Group	$P\overline{3}$ (No. 147)	$P\overline{3}$ (No. 147)
a (Å)	7.3857(4)	4.327(3)
c (Å)	10.104(1)	10.117(3)
Z	3	1

* R_p = 0.060, R_{wp} = 0.077, R_f = 0.049, R_e = 0.059 and Goodness of fit = 1.314 at 295 K.

(b)

Atom	Assignment	Occ	Site**	x	y	z	B (Å^2)
Sn		1.0	6g	0.3344(11)	0.3377(14)	0.6732(9)	3.0(1)
Rb1		1.0	1a	0.0	0.0	0.0	3.1(10)
Rb2		1.0	2d	0.3333	0.6667	−0.012(4)	4.7(6)
F1	Terminal	1.0	6g	0.291(4)	0.325(9)	0.874(2)	3.2(5)
F2	Bridge	0.9	6g	0.430(3)	0.107(4)	0.692(5)	3.2
F3	Triply bridge	0.9	2d	0.3333	0.6667	0.674(12)	3.2
F4	Triply bridge	0.9	2c	0.0	0.0	0.654(12)	3.2

** Wyckoff notation.

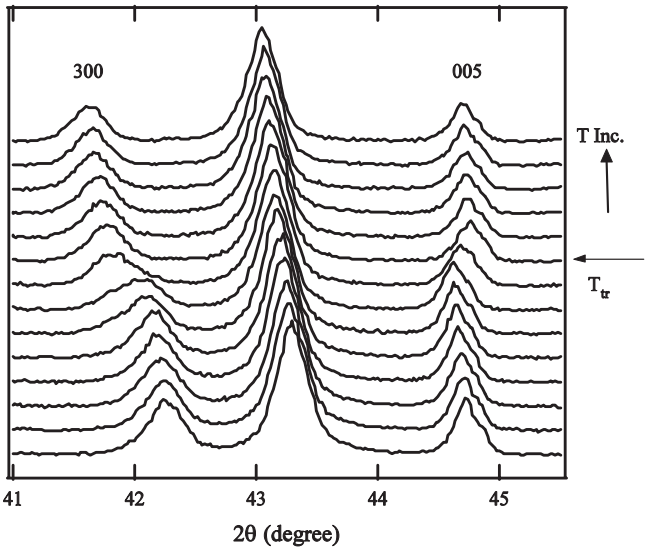

Fig. 3. Temperature dependence of the X-ray powder diffraction for $RbSn_2F_5$ at the 2θ range from 41° to 46°. 14 traces are shown from 300 K to 430 K with an interval of 10 K. Miller indices 300 and 005 are based on Phase II.

Figure 3, in which the 300 reflection shifts to the lower angle but the 005 to the higher angle. This indicates a step-wise expansion in the ab-plane and a slight contraction along the c-axis at T_{tr}. This finding is in consistent with the superionic phase of KSn_2F_5 at which a highly disordered state of the fluoride ions is formed in the two-dimensional conduction plane [23].

3.2 Impedance spectroscopy

Figure 4a shows the Cole-Cole plots of the impedance at some selective temperatures for $RbSn_2F_5$ polycrystalline sample. Below room temperature a depressed (non-ideal)

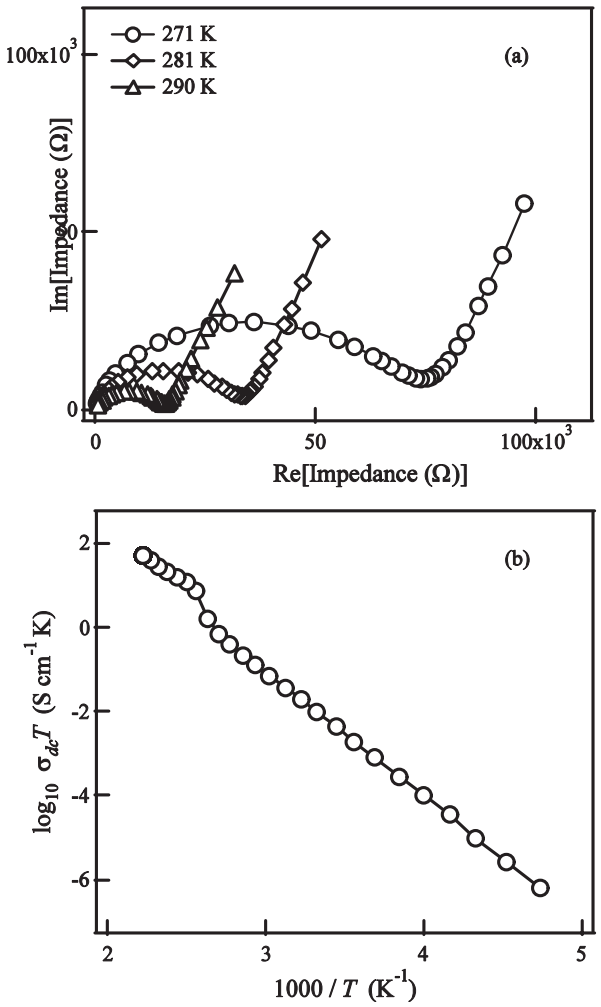

Fig. 4. (a) Cole-Cole plots of the impedance data at selected temperatures. (b) Temperature dependence of the dc ionic conductivity for $RbSn_2F_5$.

semicircle is observed accompanied by a straight line at the low frequency side suggesting an effect of the blocking electrode. Such non-ideal behavior of the impedance spectra may come from the presence of a distribution in relaxation times within the bulk response as discussed in our previous work [24].

The bulk dc conductivity $\sigma_{\rm dc}$, estimated from the Cole-Cole plots, is plotted against inverse temperature in Figure 4b. This temperature dependence was analyzed using the Arrhenius equation,

$$\sigma_{\rm dc}T = \sigma_0 \exp(-E_{\rm dc}/kT), \tag{2}$$

where σ_0 is the pre-exponential factor and $E_{\rm dc}$ is the activation energy for the ion migration. The structural phase transition from Phase II to I is confirmed by the abrupt increase of the conductivity value by about one order of magnitude. The value of the ionic conductivity reaches 0.113 $\mathrm{S\,cm^{-1}}$ at 450 K, which is in good agreement with the conductivity value measured by Hirokawa et al. [15]. The activation energies of conduction below and above the transition region were found to be 0.55 and 0.45 eV, respectively.

The frequency dependence of the real part of the conductivity, $\sigma'(\omega)$, for $RbSn_2F_5$ is shown in Figure 5a at several temperatures. At low temperatures and frequencies, random diffusion of the ionic charge carriers via activated hopping gives rise to a frequency-independent conductivity characterizes the dc conductivity $\sigma_{\rm dc}$. However, with the increase in frequency, $\sigma'(\omega)$ shows a dispersion, which shifts to higher frequencies with increasing temperature. An additional feature of $\sigma'(\omega)$, observed at high temperatures, is a decrease of $\sigma'(\omega)$ for lower frequencies below the dc conductivity due to space charge polarization at the blocking electrode.

Almond and West [25] rewrote equation (1) in the following expression to describe the frequency dependence of the bulk ac conductivity for ionic conductors

$$\sigma'(\omega) \;=\; \sigma_{\rm dc}\,[1 + (\omega/\omega_H)^n]\,, \tag{3}$$

where ω_H is the hopping frequency of the charge carriers, which represents the crossover frequency from dc to the dispersive conductivity region. The hopping frequency ω_H and the dc conductivity $\sigma_{\rm dc}$ are both thermally activated with almost the same activation energy, indicating that they are originated from the ionic migration.

The charge carriers mobility μ, is related to the hopping frequency through the Nernst-Einstein relation as

$$\mu = \frac{e}{k\,T}\,D = \frac{e}{k\,T}\,\gamma\,\lambda^2\omega_H, \tag{4}$$

where D is the diffusion coefficient, e is the electronic charge, λ the hopping distance, γ is a geometrical factor for ion hopping ($\gamma = 1/6$ for isotropic materials), and k is Boltzman's constant. Then the dc conductivity could be given by

$$\sigma_{\rm dc} = en_c\mu = \frac{n_c e^2\gamma\lambda^2}{kT}\omega_H, \tag{5}$$

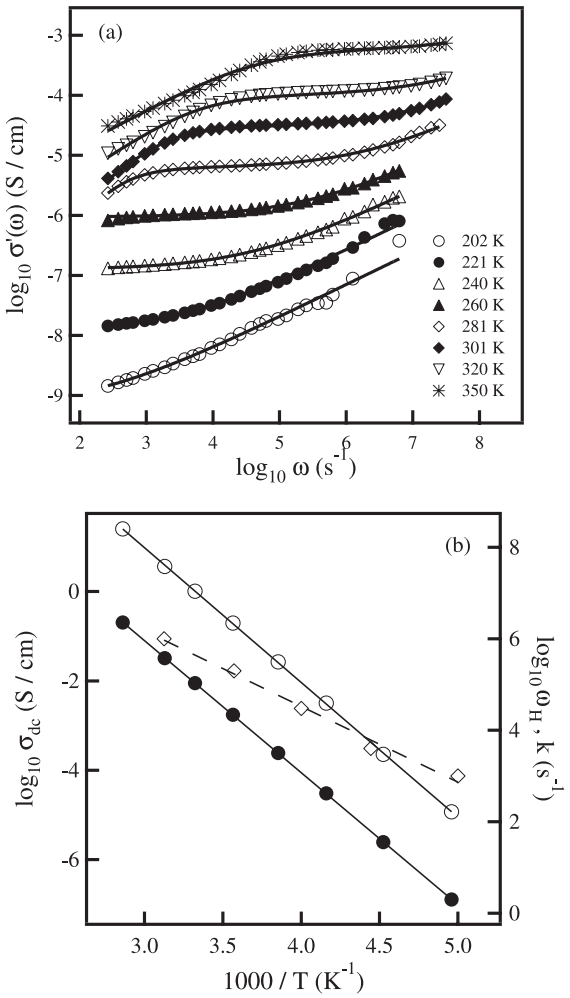

Fig. 5. (a) Conductivity spectra for $RbSn_2F_5$ at several temperatures. The solid curves are the best fits to equation (10). (b) Temperature dependence of the dc conductivity $\sigma_{\rm dc}$ (solid circle), the hopping frequency ω_H (open circle) and the exchange rate k of the NMR experiment (open diamond). Solid lines are the straight-line fits of the data.

where n_c is the concentration of mobile charge carriers. Using equation (5), equation (3) can be written in the form

$$\sigma'(\omega) \;=\; (n_c e^2\gamma\lambda^2/kT)\omega_H\,[1 + (\omega/\omega_H)^n]\,. \tag{6}$$

Both the carrier concentration n_c and the hopping frequency ω_H may be thermally activated and may be written as

$$n_c \;=\; n_0 \exp(-E_c/kT), \tag{7a}$$

and

$$\omega_H = \omega_0 \exp(-E_m/kT), \tag{7b}$$

where E_c and E_m are the creation and migration energies, respectively, of the mobile ions. It is seen from equations (6) and (7) that the activation energy for $\sigma_{\rm dc}$ is $E_\sigma \;=\; E_c + E_m$.

However, it is observed in Figure 5a that the conductivity data are highly affected by electrode polarization at

$$\sigma'_T(\omega) = \frac{Y_e\omega^a[\sigma' Y_e\omega^a + \sigma'^2\cos(a) + (2\pi\omega\varepsilon_0\varepsilon_\infty)^2\cos(a)]}{\sigma'^2 + 2Y_e\omega^a[\sigma'\cos(a) + 2\pi\omega\varepsilon_0\varepsilon_\infty\sin(a)] + (Y_e\omega^a)^2 + (2\pi\omega\varepsilon_0\varepsilon_\infty)^2}. \quad (10)$$

Table 2. Fitting parameters Y, a, $\sigma_{\rm dc}$, ω_H and n as determined from the fitting of the conductivity spectra according to equation (10). The concentration of charge carriers n_c was calculated from equation (5).

T (K)	$\log Y$ $[Hz^{-a}/(\Omega{\rm cm})]$	a	$\log\sigma_{\rm dc}$ (S/cm)	$\log\omega_H$ (s^{-1})	n	$\log n_c$ (cm^{-3})
202			−9.20	2.22	0.54	21.30
221			−7.95	3.47	0.54	21.33
240			−6.90	4.59	0.54	21.29
260			−6.03	5.50	0.54	21.30
281	−7.83	1.01	−5.21	6.34	0.56	21.30
301	−7.37	0.89	−4.53	7.04	0.55	21.32
320	−6.66	0.73	−4.00	7.58	0.55	21.34
350	−5.96	0.60	−3.24	8.41	0.56	21.31

high temperatures. Accordingly, it is necessary to include the electrode polarization effect in the fitting procedure in order to obtain reliable fitting parameters of the conductivity spectra. The electrode impedance can be modelled in terms of a complex phase element (CPE) in series with the bulk conductivity of the sample [26]. The admittance of the CPE element and the bulk complex conductivity are expressed as

$$Y^*_{CPE} = Y_e\omega^a[\cos(a) + i\,\sin(a)], \quad (8)$$

and

$$\sigma^*(\omega) = \sigma'(\omega) + i\,2\,\pi\,\omega\,\varepsilon_0\,\varepsilon_\infty, \quad (9)$$

where Y_e and a are parameters for the electrode admittance, ε_0 is the permittivity of free space, ε_∞ is the dielectric permittivity at high frequency limit, and $\sigma^*(\omega)$ is the real part of the bulk ac conductivity defined by equation (3). Then, the real part of the total complex conductivity for the bulk and the electrode is given by [26]

See equation (10) *above.*

Curve fitting were performed on the conductivity spectra according to equation (10), using Y_e, a, $\sigma_{\rm dc}$, ω_H, and n as variable parameters. Such fits at different temperatures are shown in Figure 5a and the resulting fitting parameters are listed in Table 2. The value of the dispersion exponent n is found to equal 0.55 ± 0.01. Several theoretical models have been proposed to determine the mechanism responsible for the electrical relaxation behavior in crystalline and glassy materials.

Ngai [4,27], suggested that the electrical relaxation behavior is due to the ion-ion coupling in which the motion of a mobile ion is greatly influenced by the relaxation of its neighborhood. As a result, one expected that the observed power law exponent should vary systematically with the ion concentration, i.e. the power-law exponent n should approach zero for materials with low ion concentration. On the other hand, for materials with high ionic concentration the increasing correlation among mobile ions is reflected by an increase in the exponent n.

In contrast to this picture, several studies have now shown that the power law exponent is independent of both the temperature and the mobile ion concentration. An alternative picture is that advanced by the jump relaxation model of Funke [28], in which the very motion of an ion away from its site results in a bias for the ion to return to its original site. This leads to a rapid back and forth displacement of the ion which produces sub-diffusive growth of the mean square displacement at short times. At longer times, the neighboring ions rearrange themselves (relax) with respect to the hopping ion. In this case, the bias for backward displacement is lost allowing the ion to advance successfully, resulting in a random diffusion as evidenced by the dc conductivity. Recent Monte Carlo simulations studies [29], however, revealed that the backward correlations arise from a combination of both lattice disorder and Coulomb interactions between the ions.

Sidebottom in his recent survey [30] showed that the power law exponent n for a variety of ion conducting materials is independent of both the temperature and mobile charge carriers' concentration. Instead n is found to be dependent on the dimensionality of the conduction space with a value of 0.67 for isotropic materials and relatively smaller values for low dimensional conducting materials ($n = 0.55$ for two-dimensional conductors and $n = 0.3$ for one-dimensional conductors). Accordingly, the relatively small value of the dispersion exponent ($n = 0.55$) suggests that $RbSn_2F_5$ has a 2-dimensional character, in consistence with the structure analysis as discussed above.

The temperature dependence of the hopping frequency ω_H is shown in Figure 5b, which exhibits an Arrhenius behavior described by equation (7b). The value of the activation energy, $E_m = 0.56$ eV, for the migration of charge carriers was obtained from the straight-line fit of the data in Figure 5b. E_m value is almost equal to the activation energy of the dc conductivity, $E_\sigma = 0.54$ eV, calculated from the dc conductivity data in Figure 5b. This implies that the concentration of the mobile charge carriers is weakly temperature dependent ($E_c \approx 0$) and the conductivity is determined primarily by the charge

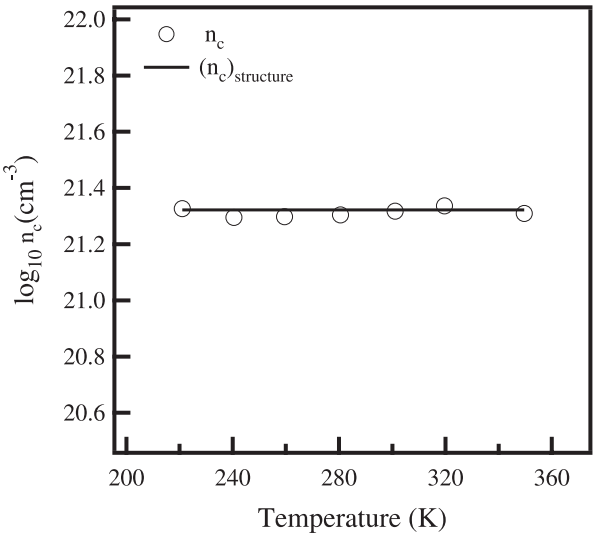

Fig. 6. Temperature dependence of the charge carriers' concentration. Solid line represents the value of n_c determined from the structure of $RbSn_2F_5$.

carriers mobility. This is in consistent with the intrinsic disordered structure at Phase II.

Using the values of $\sigma_{\rm dc}$ and ω_H, it is now possible to estimate the values of the charge carriers concentration n_c from equation (5). The value of γ in equation (5) was suggested to be equal to $1/4$ (for a two-dimensional conductor). The hopping distance λ was assumed to be 2.9×10^{-8} cm, which was estimated from the shortest F-F bond. The estimated values of n_c at different temperatures are listed in Table 2. Clearly, n_c is found to be independent of temperature in the temperature range studied, indicating an intrinsic conduction mechanism. For comparison, it is possible to determine the value of $(n_c)_{\rm structure}$ from the structure. From the structure analysis it is suggested that there is one fluoride ion vacant site per unit cell, leading to a value of $(n_c)_{\rm structure}$ of 2.10×10^{21} cm^{-3}. This value of $(n_c)_{\rm structure}$ agrees fairly well with those listed in Table 2, see also Figure 6.

3.3 Dynamic properties of the fluoride ions detected by ^{19}F, ^{119}Sn and ^{87}Rb NMR

As expected from the high ionic conductivity, the motional narrowing of the ^{19}F NMR for $RbSn_2F_5$ finished around room temperature as shown in Figure 7a. The asymmetric spectrum below 200 K could be deconvolved into three Gaussian components referring to that of the potassium salt [31]. Figure 8 shows these three components at 100 K together with that of KSn_2F_5. These three components were assigned to terminal, bridging and triply bridging fluoride ions from the high frequency side in the order of the covalent character. This assignment was based on the fact that the compactness of the valence p-electron may contribute to the paramagnetic shift. This assignment was also supported by the fact that the observed spectrum could be reproduced using the intensity ratio from the

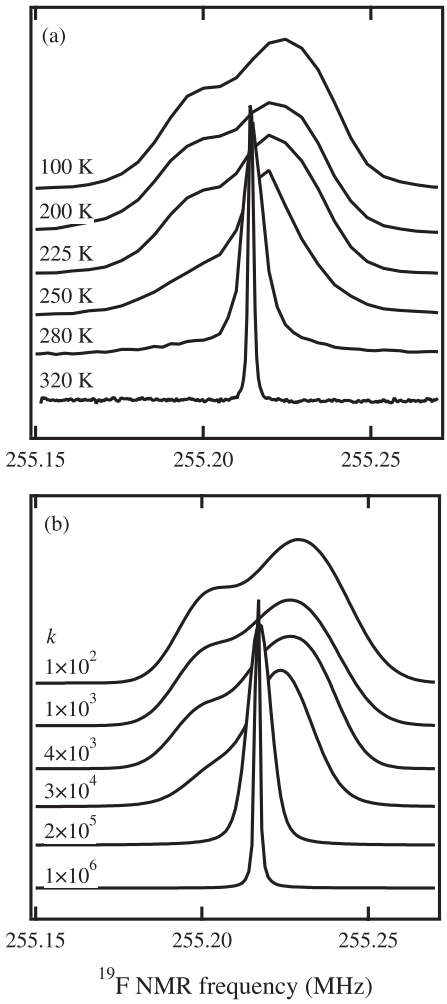

Fig. 7. (a) Temperature dependence of the ^{19}F NMR spectra of $RbSn_2F_5$ and (b) simulated spectra with the exchange rate k.

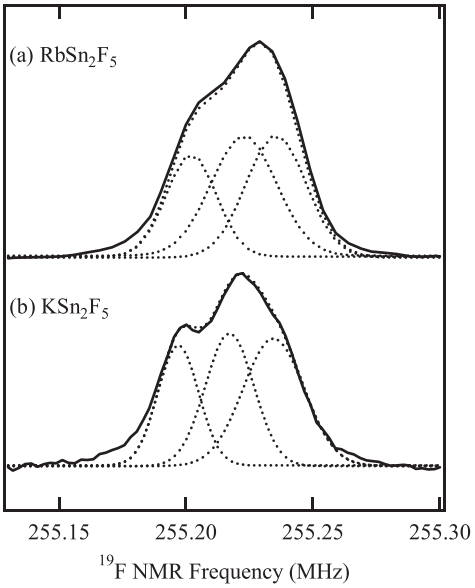

Fig. 8. ^{19}F NMR for (a) $RbSn_2F_5$ at 100 K and (b) KSn_2F_5 at 180 K. Three Gaussian components are shown by dotted lines.

structure, that is, 0.40:0.36:0.24 for terminal, bridging and triply bridging fluoride ions, respectively. With increasing temperature these three components, each of them has a width due to dipole-dipole interactions of about 25–30 kHz, collapse to a single sharp line whose position is given by the weighted-average of the three components. In this site-exchange process, the dipole-dipole interactions between nuclei are also averaged over the motion and almost vanish.

In order to estimate the exchange rate, we introduce a chemical exchange treatment. Under the three-site exchange process, the free-induction decay signal $G(t)$ followed by a single rf pulse is given by [32,33];

$$\boldsymbol{G}(t) = A\exp(i\boldsymbol{\Delta\omega}t + K - \boldsymbol{\Delta H}^2t^2)\mathbf{1} \qquad (11)$$

where $\boldsymbol{A} = (A_1, A_2, A_3)$ is a normalized intensity vector for the terminal, bridging and triply bridging sites, respectively,

$$\boldsymbol{\Delta\omega} = \begin{pmatrix} \omega_1-\omega_0 & 0 & 0 \\ 0 & \omega_2-\omega_0 & 0 \\ 0 & 0 & \omega_3-\omega_0 \end{pmatrix},$$

$$\boldsymbol{K} = \begin{pmatrix} -k_{12}-k_{13} & k_{21} & k_{31} \\ k_{12} & -k_{21}-k_{23} & k_{32} \\ k_{13} & k_{23} & -k_{31}-k_{32} \end{pmatrix},$$

$$\boldsymbol{\Delta H} = \begin{pmatrix} 1/T_{21} & 0 & 0 \\ 0 & 1/T_{22} & 0 \\ 0 & 0 & 1/T_{23} \end{pmatrix},$$

and $\mathbf{1}$ is a vector with its all components equal to unity. In these equations, $(\omega_1-\omega_0)/2\pi$ etc., are frequencies from the rf-radiation, $\boldsymbol{K}$ is the transition rate matrix defined by exchange rates k_{12} etc. $\boldsymbol{\Delta H}$ is a diagonal matrix with the Gaussian broadening parameters, $1/T_2$, for three components. We assumed $k_{12} = k_{13} = k_{23} = k$ for simplicity. Then, $\boldsymbol{K}$ matrix could be expressed using one rate constant k as,

$$\boldsymbol{K} = \begin{pmatrix} -2k & k(A_1/A_2) & k(A_1/A_3) \\ k & -k(1+A_1/A_2) & k(A_2/A_3) \\ k & k & -k(A_1+A_2)/A_3 \end{pmatrix}. \qquad (12)$$

The simulated spectrum was obtained by the Fourier transformation of $G(t)$ and then compared with the observed one. Figure 7b shows the simulations corresponding to the observation temperatures. In the temperature range from 200 to 320 K, the exchange rate could be expressed as,

$$k = 1.0\times10^{11}\ \mathrm{s}^{-1}\ \exp(-0.32\ \mathrm{eV/kT}). \qquad (13)$$

However, since NMR spectrum is more sensitive to the slow and local motion which is excited at low temperatures, the activation energy $E_{\mathrm{NMR}} = 0.32$ eV is found to be smaller than that of the conductivity data, $E_{\mathrm{dc}} = 0.55$ eV. This activation energy from the NMR measurements may represent the microscopic activation energy of the localized motion of fluoride ions.

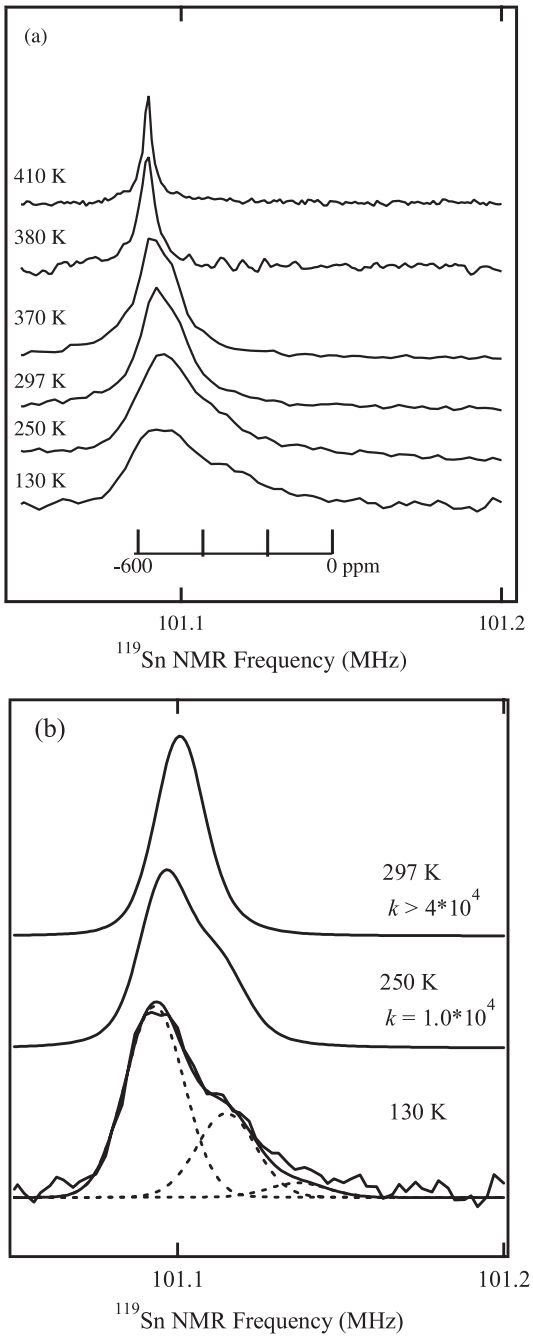

Fig. 9. (a) Temperature dependence of the ^{119}Sn NMR spectra of $RbSn_2F_5$. $(CH_3)_4Sn$ was used as a chemical shift standard. (b) Deconvolution into three components at 130 K and the simulations according to equation (12).

^{119}Sn NMR is a valuable technique to characterize this fluoride ion conductor, $RbSn_2F_5$. Figure 9a shows a characteristic change of the ^{119}Sn NMR spectra as a function of temperature. At temperatures below 250 K, the spectrum consists of more than two components with a main peak at −530 ppm and a second rather broad one *ca.* −350 ppm. With increasing temperature the second component shifts to the low frequency side with decreasing its intensity. This component almost disappears

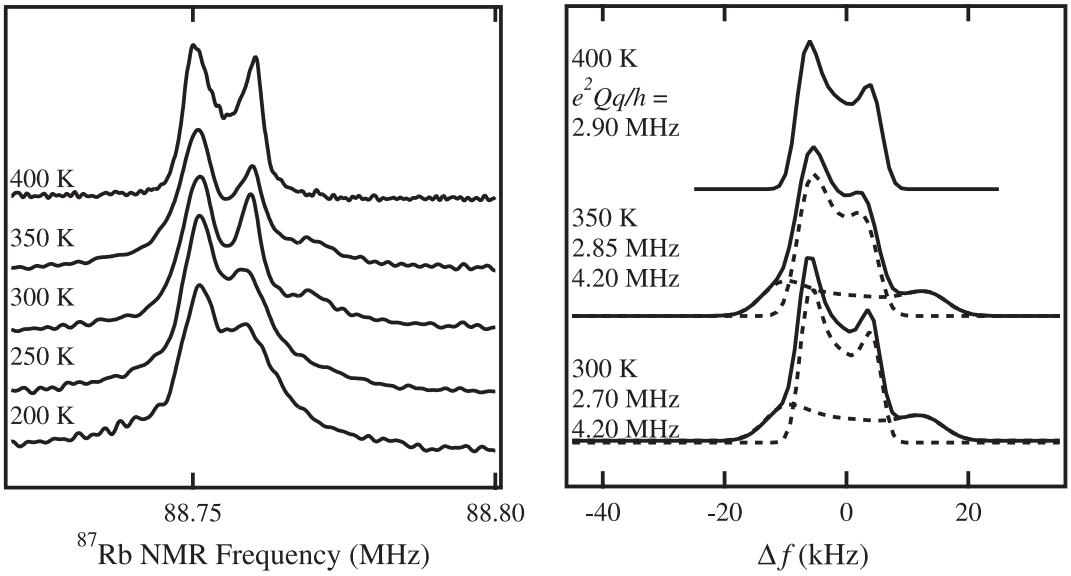

Fig. 10. (a) ^{87}Rb NMR spectra of $RbSn_2F_5$ at selective temperatures. (b) Simulated ^{87}Rb NMR spectra and quadrupole coupling constants above 300 K using a second order quadrupole effect.

at 297 K at which the ^{19}F NMR spectrum attains the motional narrowing completely. The asymmetric spectrum below 250 K looks like a anisotropic powder pattern having an axial symmetric chemical shift. However, since stoichiometric $RbSn_2F_5$ contains intrinsic vacancies at the site of the fluoride ions, we explain the asymmetric spectrum as a result of the superposition of several components neglecting the chemical shift anisotropy of each component. If we introduce the occupancies of the fluoride ions according to Table 1, the probability of the tin environment with N legends, $P(N)$, could be estimated as a binomial distribution,

$$P(N) =_4 C_{n-1}(p)^{N-1}(1-p)^{5-N}, \qquad (14)$$

where $1 \leq N \leq 5$ and $p(= 0.90)$ is an occupancy at F2, F3 and F4 sites, whereas F1 site is fully occupied. The calculated intensity ratio for $P(5)$:$P(4)$:$P(3)$ is 0.66:0.29:0.05 which can reproduce the ^{119}Sn NMR spectrum at 130 K successfully as shown in Figure 9b. Similar to the chemical exchange phenomenon observed for the ^{19}F NMR, we tried to simulate the ^{119}Sn NMR spectra using equation (12). As Figure 9b shows, we could reproduce the observed one except the sharp component which appeared above 297 K.

According to our previous works on the perovskite related $RSnCl_3$ (R = Cs and alkylammonium), the isotropic chemical shift of the ^{119}Sn NMR increases its frequencies with the cationic radius due to the appearance of the isolated $SnCl_3^-$ anion [34]. Therefore, the shoulder at the high frequency side may suggest the existence of the Sn^{2+} with a lower coordination number. On the other hand, a sharp component appears above T_{tr} accompanied by a step-wise decrease of the peak frequency. This change may suggest a rapid diffusion of the fluoride ions and also suggest the increased ionicity of the Sn-F bonds as is expected from Figure 3.

Figure 10a shows the ^{87}Rb NMR spectra for $RbSn_2F_5$ at selective temperatures. As expected from the large quadrupole moment with a nuclear spin $I = 3/2$, a second order quadrupole effect was observed on the central transition ($m = -1/2 \leftrightarrow 1/2$) over the whole temperature range studied. ^{87}Rb NMR spectrum above T_{tr} shows single component with an axial symmetric ($\eta = 0$) quadrupole interaction as is expected from the structure. Below T_{tr}, however, at least two components overlap each other. Figure 10b shows the simulated powder patterns with the quadruple coupling constants used. Although two components with intensity ration 2:1 could be seen clearly at 350 and 300 K, we could not decide the number of the Rb sites below 250 K, at which anionic sublattice forms a rigid lattice. This is probably due to the random distribution of the fluoride ion vacancies similar to the ^{119}Sn spectrum below 250 K.

4 Conclusions

We have studied the ionic conduction and relaxation in $RbSn_2F_5$ by impedance spectroscopy and NMR measurements. The two-dimensional structure at phase II was determined from Rietveld analysis of X-ray diffraction data and the reduction of the unit cell from $Z = 3$ to 1 was also confirmed at 368 K accompanied by an expansion along the *ab*-plane and a construction along *c*-axis. The dc conductivity and conductivity relaxation of $RbSn_2F_5$ have been studied in wide ranges of frequencies and temperatures. An abrupt increase in the conductivity value confirms the superionic transition.

We have estimated the hopping frequency of the charge carriers and its respective activation energy from the analysis of the conductivity spectra using Almond-West formalism. The activation energies for the dc conductivity and the hopping frequency are almost equal, 0.55 ± 0.01 eV, suggesting weakly temperature dependence of the charge carriers' concentration, which implies that the conductivity arises from the mobility of the charge carriers. The estimated values of n_c determined from the analysis of the conductivity spectra by Almond-West formalism are found to be independent of temperature and agree well with that determined from the structure, suggesting that ω_H may represent the real hopping frequency of mobile ions.

^{19}F NMR spectra exhibit the site-exchange phenomena associated with the narrowing below room temperature, suggesting that all the fluoride ions contribute to the high conductivity of this material. ^{119}Sn and ^{87}Rb NMR spectra support the intrinsic disordered structure at Phase II and suggest the appearance of the averaged structure above T_{tr}.

References

1. D. Brinkmann, Progr. NMR Spectrosc. **24**, 527 (1992)
2. S. Martin, Mater. Chem. Phys. **23**, 225 (1989), and references therein
3. C.A. Angell, Solid State Ionics **18/19**, 72 (1985)
4. K.L. Ngai, Comments Solid State Phys. **9**, 127 (1979); K.L. Ngai, Comments Solid State Phys. **9**, 141 (1980)
5. A. Pradel, M. Ribes, J. Non-Cryst. Solids **131–133**, 1063 (1992)
6. A.K. Jonscher, *Dielectric Relaxation in Solids* (Chelsia Dielectric, London, 1983)
7. A.K. Jonschor, Nature (London) **267**, 673 (1977)
8. D.P. Almond, A.R. West, J. Non-Cryst. Solids **88**, 222 (1986)
9. J. Dyre, J. Non-Cryst. Solids **153**, 219 (1991)
10. S.R. Elliott, J. Non-Cryst. Solids **170**, 97 (1994)
11. B. Roling, A. Happe, K. Funke, M. D. Ingram, Phys. Rev. Lett. **78**, 2160 (1997)
12. D.L. Sidebottom, P.F. Green, R.K. Brow, Phys. Rev. B **56**, 170 (1997)
13. B. Roling, Solid State Ionics **105**, 185 (1998)
14. W.D. Basler, I.V. Murin, S.V. Chernov, Z. Naturforsch. a **36**, 519 (1981)
15. K. Hirokawa, H. Kitahara, Y. Furukawa, D. Nakamura, Ber. Bunsenges. Phys. Chem. **95**, 651 (1991)
16. G. Bergerhoff, H. Namgung, Acta Crystallogr. B **34**, 699 (1978)
17. R.R. MacDonald, A.C. Larson, D.T. Cormer, Acta Crystallogr. **17**, 1104 (1964)
18. J.P. Battut, J. Dupuis, S. Soudani, W. Granier, S. Vilminot, H. Wahbi, Solid State Ionics **22**, 247 (1987)
19. S. Vilminot, R. Bachmann, H. Schulz, Solid State Ionics **9/10**, 559 (1983)
20. F. Izumi, T. Ikeda, Mater. Sci. Forum **321–324**, 198 (2000)
21. MathSoft International, Knightway House, Park Street, Bagshot Surrey, GU19 5AQ, United Kingdom
22. S. Vilminot, H. Schulz, Acta Crystallogr. B **44**, 233 (1988)
23. K. Yamada, M.M. Ahmad, H. Ohki, T. Okuda, H. Ehrenberg, H. Fuess, Solid State Ionics **167**, 301 (2004)
24. M.M. Ahmad, K. Yamada, T. Okuda, J. Phys.: Condens. Matter **14**, 7233 (2002)
25. D.P. Almond, A.R. West, Nature **306**, 456 (1983); D.P. Almond, G.K. Ducan, A.R. West, Solid State Ionics **8**, 159 (1983); J. Non-Cryst. Solids **74**, 285 (1985); D.P. Almond, A.R. West, R. Grant, Solid State Commun. **44**, 1277 (1982)
26. E.F. Hairetdinov, N.F. Uvarov, H.K. Patel, S.W. Martin, Phys. Rev. B **50**, 13259 (1994)
27. K.L. Ngai, R.W. Rendell, H. Jain, Phys. Rev. B **30**, 2133 (1984)
28. K. Funke, Prog. Solid State Chem. **22**, 111 (1993)
29. P. Maass, M. Meyer, A. Bunde, Phys. Rev. B **51**, 8164 (1995)
30. D.L. Sidebottom, Phys. Rev. Lett. **83**, 983 (1999)
31. T. Okuda, K. Saisho, Y. Ogiso, K. Yamada, J. Chikami, G. Miehe, H. Ehrenberg, H. Fuess, *in Proceedings of the 7th Asian Conference on Solid State Ionics, Materials and Devices*, *Fuzhou*, 2000, edited by B.V.R. Chowdari, W. Wang (World Scientific, Fuzhou, 2000), p. 33
32. K. Schmidt-Rohr, H.W. Spiess, *Multidimensional Solid-State NMR and Polymers* (Academic Press, London, 1994)
33. A. Abragam, *Principles of Nuclear Magnetism* (Oxford University Press, London, 1961), Chap. X
34. H. Yano, Y. Furukawa, Y. Kuranaga, K. Yamada, T. Okuda, J. Mol. Struct. **520**, 173 (2000)